NATIONAL ADVISORY COMMITTEE FOR AERONAUTICS

TECHNICAL NOTE 3449

THEORETICAL ANALYSIS OF INCOMPRESSIBLE FLOW THROUGH A RADIAL-INLET CENTRIFUGAL IMPELLER AT VARIOUS WEIGHT FLOWS

II - SOLUTION IN LEADING-EDGE REGION BY RELAXATION METHODS

By James J. Kramer

Lewis Flight Propulsion Laboratory
Cleveland, Ohio

Washington
June 1955

NATIONAL ADVISORY COMMITTEE FOR AERONAUTICS

TECHNICAL NOTE 3449

THEORETICAL ANALYSIS OF INCOMPRESSIBLE FLOW THROUGH A RADIAL-INLET CENTRIFUGAL IMPELLER AT VARIOUS WEIGHT FLOWS

II - SOLUTION IN LEADING-EDGE REGION BY RELAXATION METHODS

By James J. Kramer

SUMMARY

The detailed solution of the flow around the blade nose of a 48-inch-diameter radial-inlet centrifugal impeller has been obtained by relaxation methods for four weight flows. The results are presented in a series of figures showing streamlines and relative velocity contours. Minimum velocity gradients around the blade nose occurred for the weight flow corresponding to a mean angle of attack of -4.6° computed from blade speed and an upstream axial-radial velocity for which blade blockage has been taken into account. A small positive local angle of attack seems desirable for blades with rounded leading edges.

INTRODUCTION

In reference 1, a method for the solution of the flow through a centrifugal impeller was described and applied to an impeller similar to that described in references 2 and 3. The resulting solution was then used to check the accuracy of the approximate method described in reference 4, especially in the inlet region. More detailed information concerning the flow behavior near the leading edge than that obtained in the original solution is desirable because a knowledge of the velocity gradients in this region is helpful in avoiding boundary-layer separation caused by rapidly decelerating flow. The magnitude of losses caused by boundary-layer separation at the leading edge is discussed in references 5 and 6 for sharp-nosed blades, but the manner in which the losses occur is not discussed.

The solution was, therefore, refined in the nose region by solving for the stream function with the use of a grid of much finer mesh size than that used in the original problem. This extension is dependent on the original solution because the refinement is obtained in a region along whose boundaries the values of the stream function are known from the original solution.

ANALYSIS

Statement of Problem

The flow patterns for four weight flows at an operating tip speed of 700 feet per second for nonviscous, incompressible flow in a radial-inlet centrifugal impeller were presented in reference 1. However, the information obtained concerning the flow about the leading edge was not sufficiently detailed. Therefore, the solutions for the four weight flows were refined in the region of the leading edge by solving the partial differential equation by numerical methods with a grid of considerably finer mesh. The impeller investigated, similar to that described in references 2 and 3, had a 48-inch diameter and 18 blades. The sharp leading edge and blunt trailing edge of the test impeller were rounded for the theoretical solutions in order to reduce the number of grid points necessary to define the leading-edge shape. The blades are shown in the radial-tangential plane in figure 1 and the view in the axial-radial plane is shown in figure 2. The modified blade coordinates are given in table I of reference 1. The procedure used to refine the flow solution around the blade nose is outlined in the following sections.

Assumptions. - The flow is assumed to be steady, nonviscous, and incompressible. The region in which the flow pattern is to be studied more carefully is outlined by the bold lines in figure 1. These boundary lines are chosen sufficiently far from the blade, so that the process of obtaining the refined solution does not significantly affect the conditions along the boundaries as defined by the original solution (ref. 1). Experience has shown that the distance between these boundaries and the enclosed body should be two to three times the thickness of the enclosed body. The assumption is then made that the values of the stream functions along these boundaries can be considered known and equal to the values obtained in the original solution along these lines.

Equations. - The definitions, symbols, and equations governing the flow are the same as in reference 1, but are repeated herein for convenience. The solution is obtained on a surface of revolution generated by the mean blade-height line. The trace of this surface in the axial-radial plane is approximated by the following function:

$$z = \frac{-0.041456}{(r - 0.40828)} + \text{constant} \qquad (1)$$

where r and z are cylindrical coordinates. All symbols are defined in the appendix.

Although the solution is obtained on a surface, a variation in stream-sheet thickness (normal to the z-axis) is considered. For this problem, the stream-sheet thickness was taken as the blade height (normal to the z-axis) and approximated with negligible error by the following equation:

$$b = 0.07208 + 1.01517\, e^{-1.54601r}$$

The stream function Ψ is defined by the following equations:

$$\left.\begin{aligned} \frac{\partial \Psi}{\partial r} &= -b\rho w_\theta \\ \frac{\partial \Psi}{\partial \theta} &= rb\rho w_r \end{aligned}\right\} \tag{2}$$

where θ is the angular cylindrical coordinate of a right-handed system, w_r and w_θ are relative velocity components in the r- and θ-directions, respectively, and ρ is the fluid density. The differential equation governing the flow in terms of the stream function under the previously stated assumptions is

$$\frac{\partial^2 \Psi}{dr^2} + \left(\frac{1}{r} - \frac{\partial \ln b}{\partial r}\right)\frac{\partial \Psi}{\partial r} - \frac{1}{r^2}\left(1 + \frac{1}{\lambda^2}\right)\frac{\partial^2 \Psi}{\partial \theta^2} = 2\omega b\rho \tag{3}$$

where ω is the angular velocity of the impeller and λ is equal to dr/dz along the surface. This derivative, which can be obtained from equation (1), is

$$\frac{1}{\lambda} = \frac{0.041456}{(r - 0.40828)^2}$$

Equation (3) governs the flow and, together with the boundary conditions, determines the problem mathematically.

Boundary conditions. - The boundary conditions are obtained from the original solution. The value of the stream function, expressed as a dimensionless ratio of the weight flow through a single passage, on the blade surface is equal to zero; the values along the other boundaries are obtained from cross plots of the original data (ref. 1). The error involved in reading values from the cross plots was less than 0.0003 with values of Ψ/M ranging from 0 to 1.0.

Method of Solution

Relaxation method. - The solution of equation (3) was obtained by means of relaxation techniques (ref. 7). The residuals of the relaxation process were reduced to a value indicating unit change in the fifth decimal place of the stream function. This degree of accuracy is consistent with the accuracy of the cross plots used to obtain the boundary values.

Grid. - The grid used in the relaxation process is shown in figure 3. The density of the grid lines is greatest in the region of the leading edge and decreases gradually in both directions. This type of grid

assured greatest accuracy in the region of main interest. The ratio of the grid spacing in either direction at a point is never greater than 2.5 and usually less than or equal to 2.0. The intersections of the grid lines are called grid points. The grid points in the interior of the boundaries are the points at which the numerical solution is obtained. There were 138 interior grid points for this problem.

Finite-difference approximation. - The derivatives of equation (3) were written in finite-difference form with a three-point system used, that is, with a parabolic variation assumed between grid points. In the original solution a five-point system was used. Because of the fineness of the grid, a three-point system was considered adequate for this problem.

RESULTS AND DISCUSSION

The results of the numerical procedure are presented in figures 4 and 5, which show streamlines (contours of constant Ψ/M) and contours of constant ratio of relative velocity to tip speed, respectively. Figures 4 and 5 are projections on the polar-coordinate plane. The solutions for four weight flows, the same as those of reference 1, are designated as in the following table:

Case	Weight flow, lb/sec
A	14
B	26.25
C	32.10
D	44

Streamlines

The streamlines, in general, are smooth curves. This result indicates that a sufficiently fine grid was used in the region of large variations.

The stagnation point shifts from the driving face to the trailing face as the weight flow increases from 14 to 44 pounds per second. The radial position of the stagnation point varies from $r \sim 1.05$ to $r \sim 1.028$. The relatively close spacing in the radial direction of the streamlines for case A is caused by the low weight flow. This spacing increases as the weight flow increases. Although the relative tangential velocity just upstream of the blade row is the same for all weight flows, the radial spacing of the streamlines changes because of the manner in which the stream function is made dimensionless in the figure

presentation. Ten percent of the weight flow through a single passage occupies each stream tube for all the examples, so that, in a comparison of the solutions for various weight flows, it should be noted that the weight flow through a single stream tube is directly proportional to the total weight flow. The streamlines adjacent to the nose curve sharply for case A. The curvature for case D is not so pronounced because of the wider radial spacing of the streamlines.

Velocities

Contours of constant ratio of relative velocity to tip speed (tip speed of 700 ft/sec for all four weight flows) are shown in figure 5. For case A (fig. 5(a)), there is a rapid local acceleration around the nose followed by a less rapid deceleration on the trailing face. The effect of the eddy attached to the driving face (see ref. 1) is manifested in the almost constant low velocity along the driving face. For case D (fig. 5(d)), the very rapid local acceleration followed by the less rapid deceleration occurs on the driving face. The peak velocity is greater for case D than for case A, and the subsequent deceleration is probably more serious than for the lower weight flow because the low-momentum air caused by the deceleration aggravates the secondary-flow conditions. These secondary flows transport the low-momentum fluid on the driving face to the trailing face. This type of motion is discussed in more detail in reference 8.

For case B a slight deceleration occurs on the driving face. As pointed out in reference 1, the weight flow of 26.25 pounds per second is that for which a mean angle of attack of -4.6° occurs when computed from the weight flow, rotational speed, and inlet annular area with blade blockage taken into account. The mean angle of attack is the angle between the tangent to the blade mean line at the leading edge and the mean flow direction. The sign convention for angle of attack, shown in figure 3, is chosen so that flow directed at the driving face results in a positive angle of attack. The weight flow of 26.25 pounds per second is also that corresponding experimentally to maximum efficiency. However, since the leading edge was rounded, the experimental results cannot be explained in terms of the exact solution. For the solution of case B, the local angle of attack, that is, the angle between the tangents to the blade mean line and the stagnation streamline, is approximately $+6^\circ$, whereas for case C the local angle of attack is -7°. Thus, the weight flow for zero local angle of attack is about 29 pounds per second. However, zero local angle of attack is not necessarily desirable for rounded leading edges such as the one considered herein. In view of the velocity contours of the 26.25- and 32.10-pound-per-second cases, a slight positive local angle of attack seems desirable. For a weight flow of 29 pounds per second a greater deceleration would probably occur on the driving face than that which occurs for

26.25 pounds per second. This appears to be the case since the leading edge is shaped so that at zero local angle of attack the flow on the blade surfaces would be roughly symmetrical about the blade mean line. Consequently, it seems advisable to design the leading-edge regions in the manner suggested in reference 9 and further discussed in reference 10. These leading-edge regions are characterized by very little curvature of the driving face so that flow alined with the driving face would produce little or no local deceleration.

SUMMARY OF RESULTS

The detailed solution of the flow around the blade nose of a 48-inch-diameter radial-inlet centrifugal impeller was obtained by means of relaxation techniques. The results are presented in a series of figures showing streamlines and contours of constant resultant velocity ratio. The following results were noted:

1. The stagnation point shifted from the driving to the trailing face of the blade as the weight flow increased. The total shift in the radial direction was approximately 0.02 foot.

2. Minimum velocity gradients around the blade nose occurred for the weight flow corresponding to an angle of attack of -4.6° computed from blade speed and an upstream radial-axial velocity for which blade blockage has been taken into account.

3. A small positive local angle of attack seems desirable for rounded leading-edge blades.

National Advisory Committee for Aeronautics
Lewis Flight Propulsion Laboratory
Cleveland, Ohio, March 4, 1955

APPENDIX - SYMBOLS

The following symbols are used in this report:

b	stream-sheet thickness in z-direction, ft
M	weight flow through single passage, lb/sec
r	radial distance, ft
W	ratio of relative velocity to tip speed
w	relative velocity, ft/sec
z	axial distance, ft
θ	angular coordinate, radians
λ	slope of trace of stream surface in axial-radial plane
ρ	fluid density, lb/cu ft
Ψ	stream function, eq. (2)
ω	angular velocity of impeller, radian/sec

Subscripts:

r	component in radial direction
t	tip
θ	component in tangential direction

REFERENCES

1. Prian, Vasily D., Kramer, James J., and Wu, Chung-Hua: Theoretical Analysis of Incompressible Flow Through a Radial-Inlet Centrifugal Impeller at Various Weight Flows. I - Solution by a Matrix Method and Comparison with an Approximate Method. NACA TN 3448, 1955.

2. Michel, Donald J., Ginsburg, Ambrose, and Mizisin, John: Experimental Investigation of Flow in Rotating Passages of a 48-Inch Impeller at Low Tip Speeds. NACA RM E51D20, 1951.

3. Prian, Vasily D., and Michel, Donald J.: An Analysis of Flow in Rotating Passage of Large Radial-Inlet Centrifugal Compressor at Tip Speed of 700 Feet Per Second. NACA TN 2584, 1951.

4. Stanitz, John D., and Prian, Vasily D.: A Rapid Approximate Method for Determining Velocity Distribution on Impeller Blades of Centrifugal Compressors. NACA TN 2421, 1951.

5. Kramer, James J., and Stanitz, John D.: Prediction of Losses Induced by Angle of Attack in Cascades of Sharp-Nosed Blades for Incompressible and Subsonic Compressible Flow. NACA TN 3149, 1955.

6. Wright, Linwood C.: Approximate Effect of Leading-Edge Thickness, Incidence Angle, and Inlet Mach Number on Inlet Losses for High-Solidity Cascade of Low Cambered Blades. NACA TN 3327, 1954.

7. Southwell, R. V.: Relaxation Methods in Theoretical Physics. Clarendon Press (Oxford), 1946.

8. Hamrick, Joseph T., Mizisin, John, and Michel, Donald J.: Study of Three-Dimensional Internal Flow Distribution Based on Measurements in a 48-Inch Radial-Inlet Centrifugal Impeller. NACA TN 3101, 1954.

9. Weinig, F.: Die Strömung um die Schaufeln von Turbomachinen. Johann Ambrosius Barth (Leipzig), 1935.

10. Stanitz, John D.: Effect of Blade-Thickness Taper on Axial-Velocity Distribution at the Leading Edge of an Entrance Rotor-Blade Row with Axial Inlet, and the Influence of This Distribution on Alinement of the Rotor Blade for Zero Angle of Attack. NACA TN 2986, 1953.

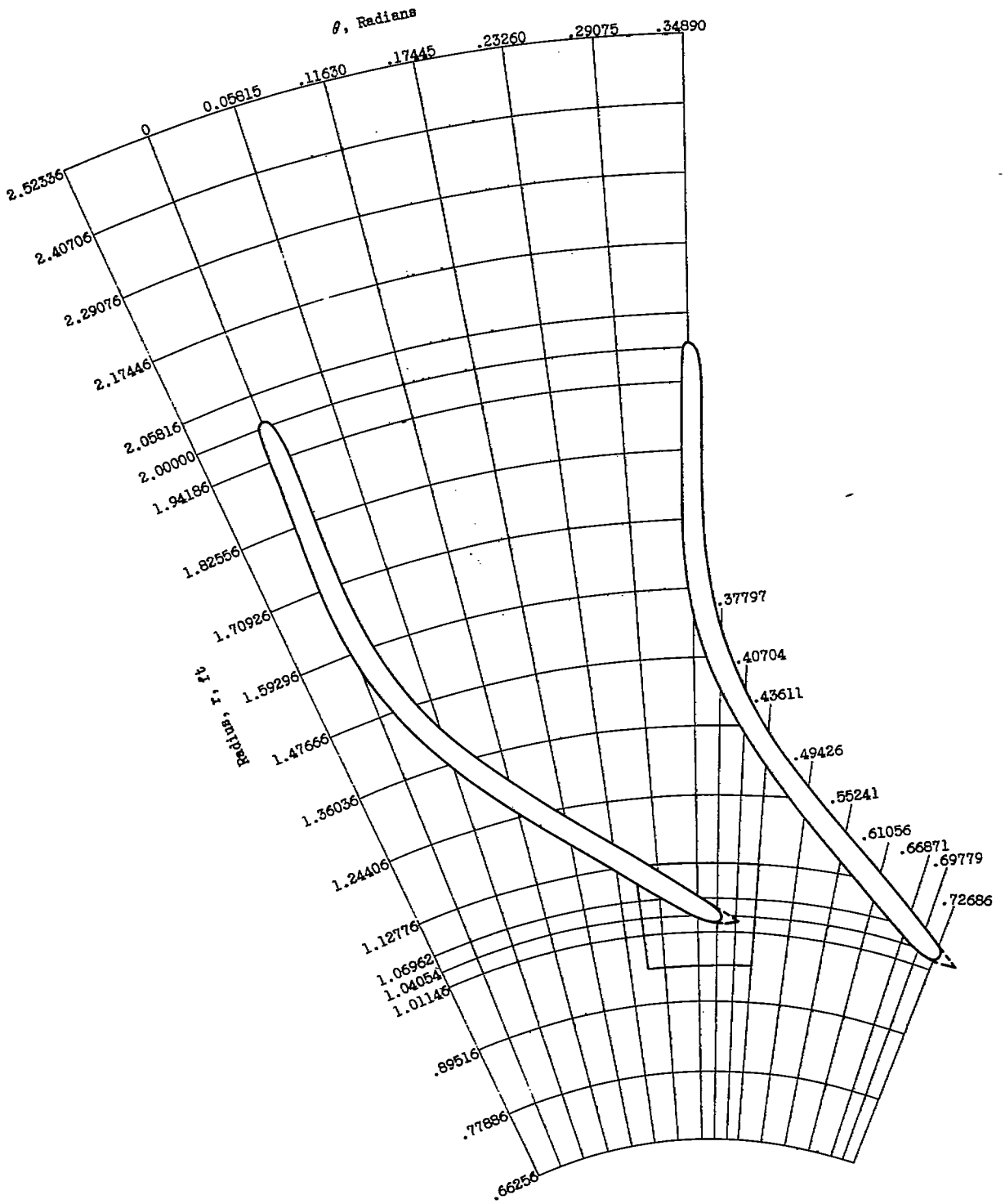

Figure 1. - Grid system for over-all solution.

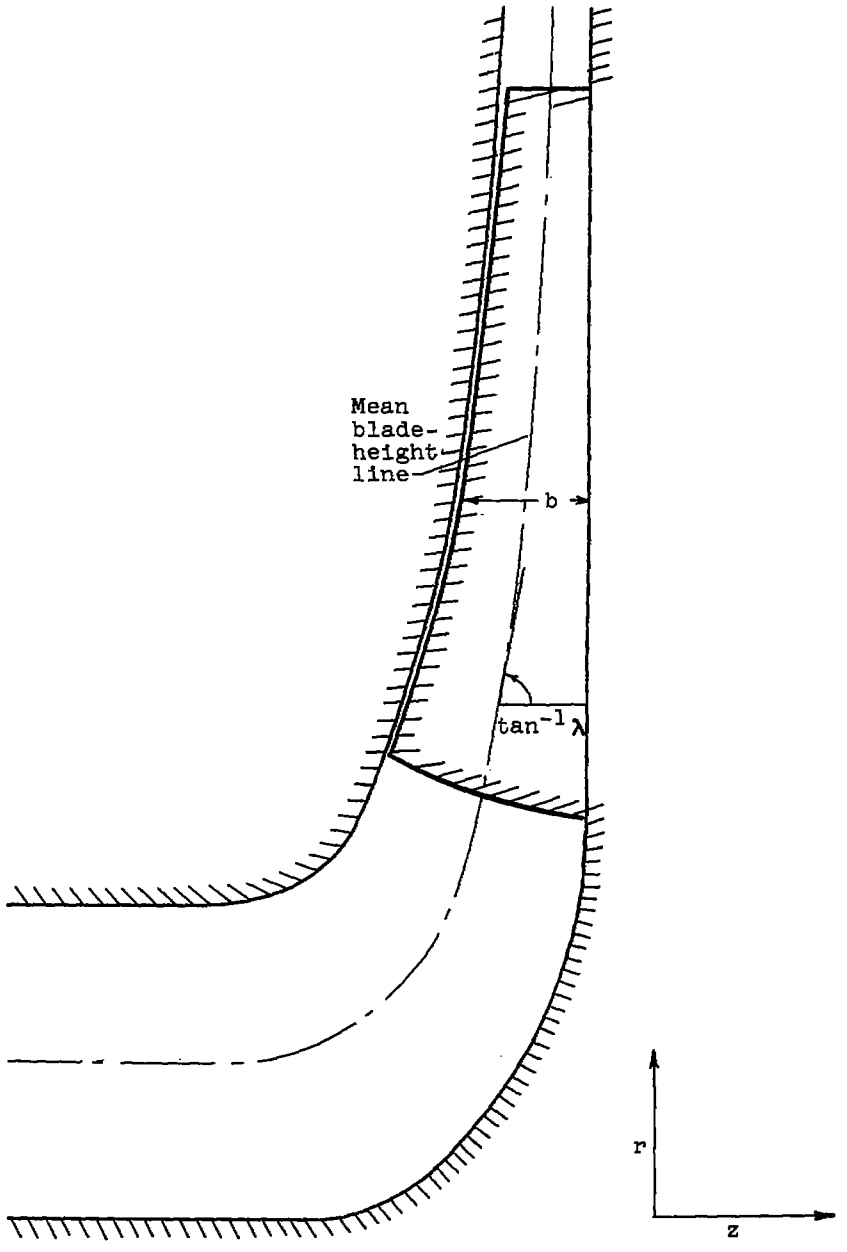

Figure 2. - Axial-radial plane view of 48-inch-diameter centrifugal impeller.

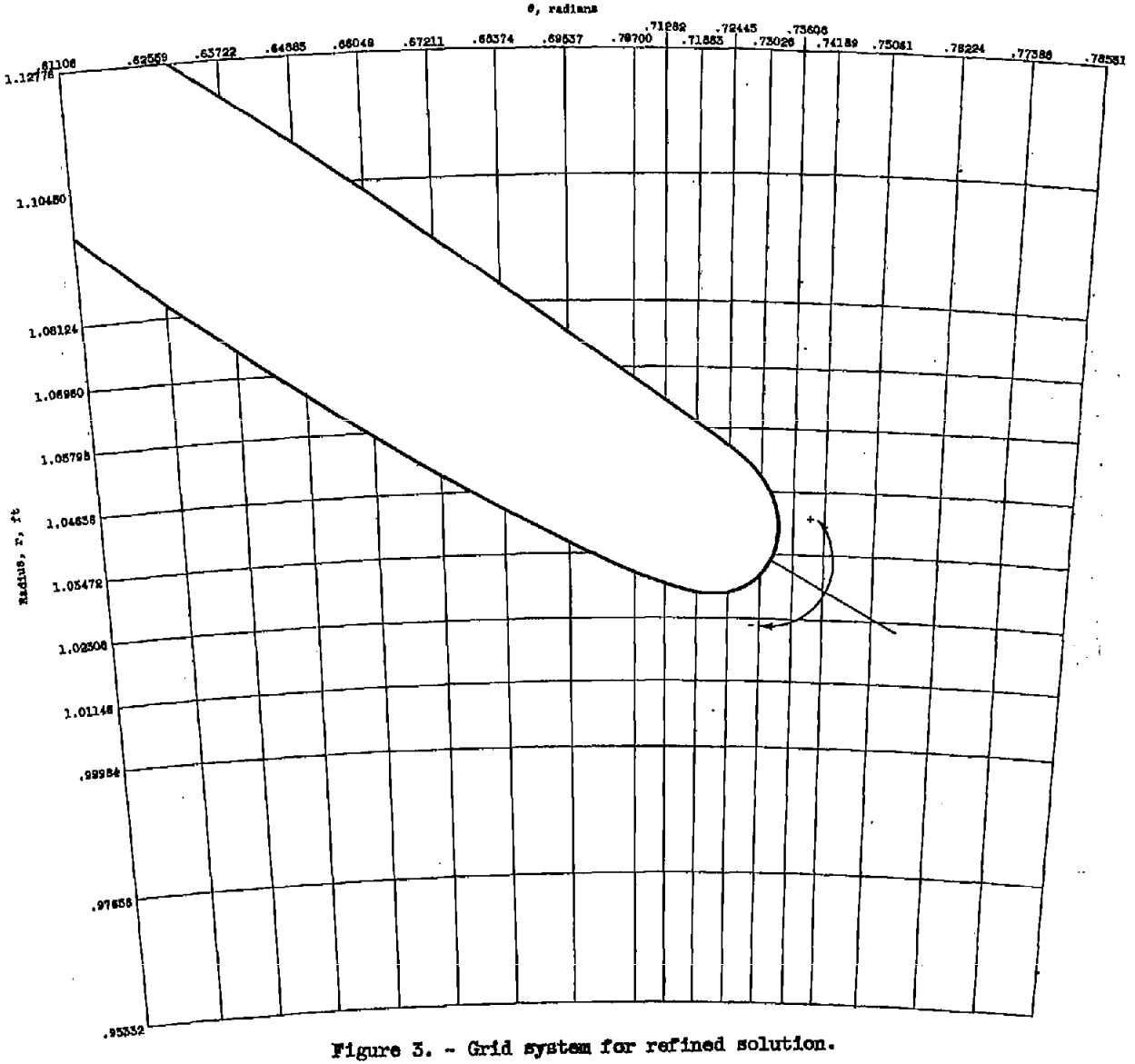

Figure 3. - Grid system for refined solution.

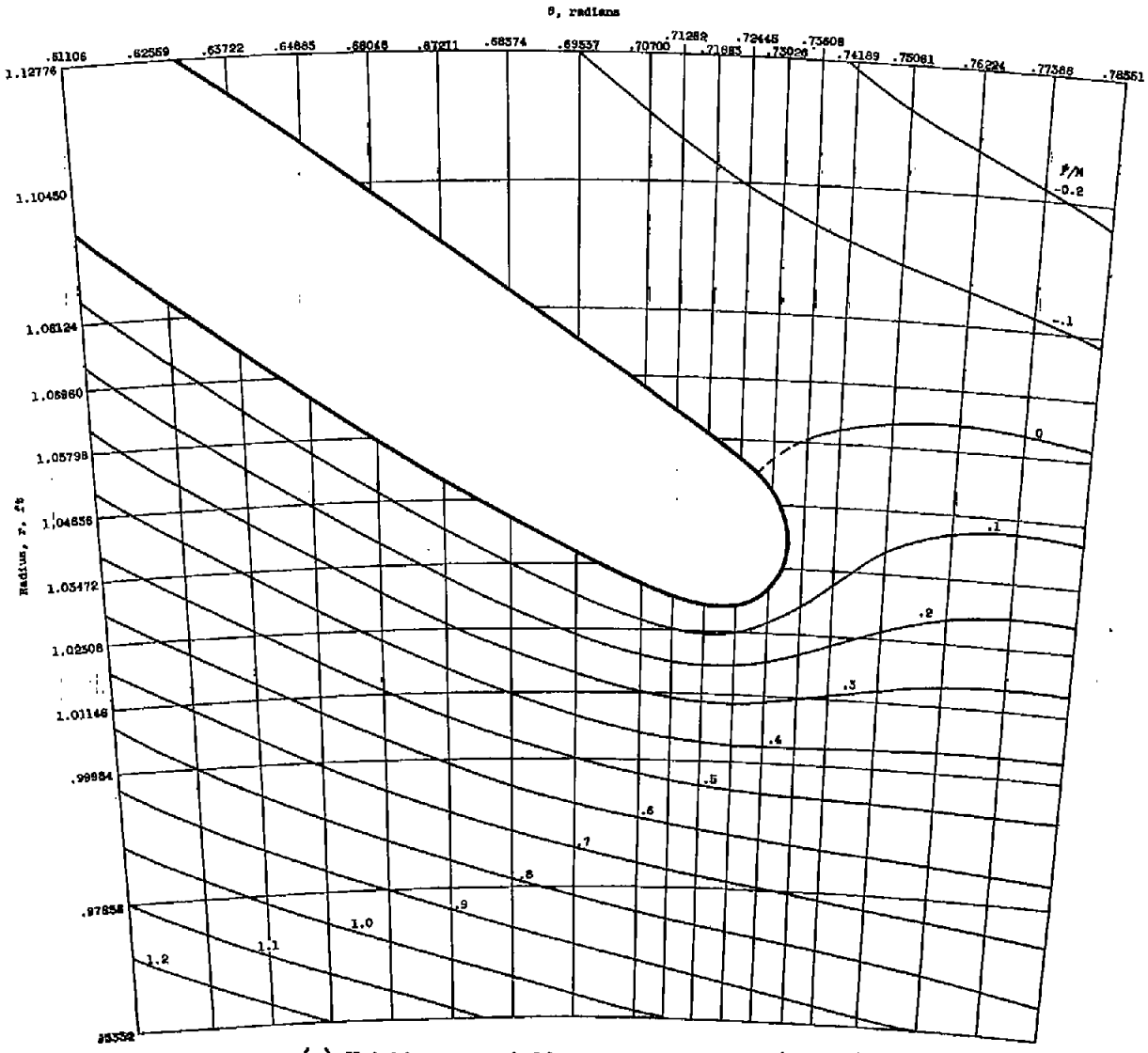

(a) Weight flow, 14.00 pounds per second (Case A).

Figure 4. - Streamlines for refined solution in nose region.

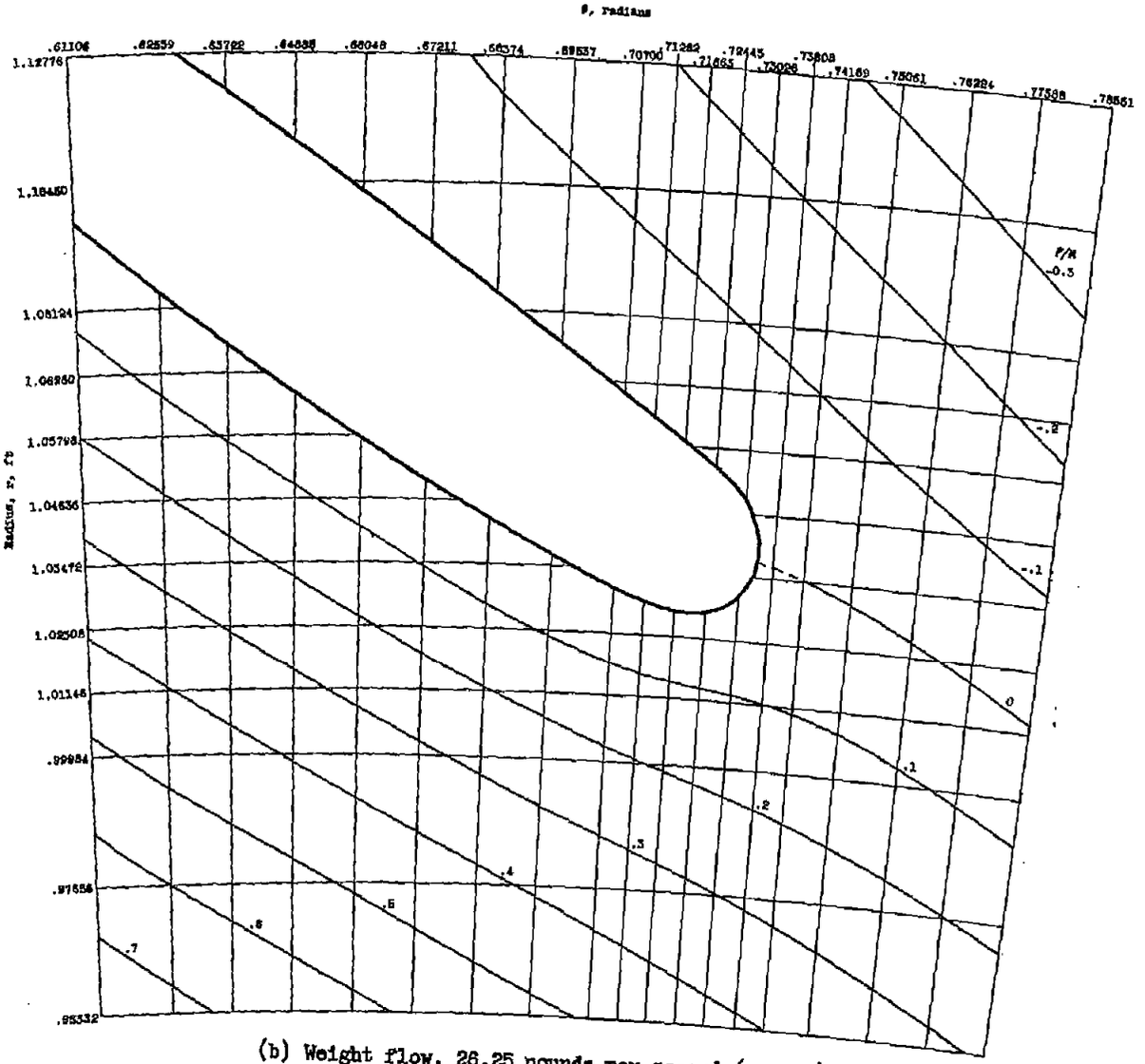

(b) Weight flow, 26.25 pounds per second (case B).

Figure 4. - Continued. Streamlines for refined solution in nose region.

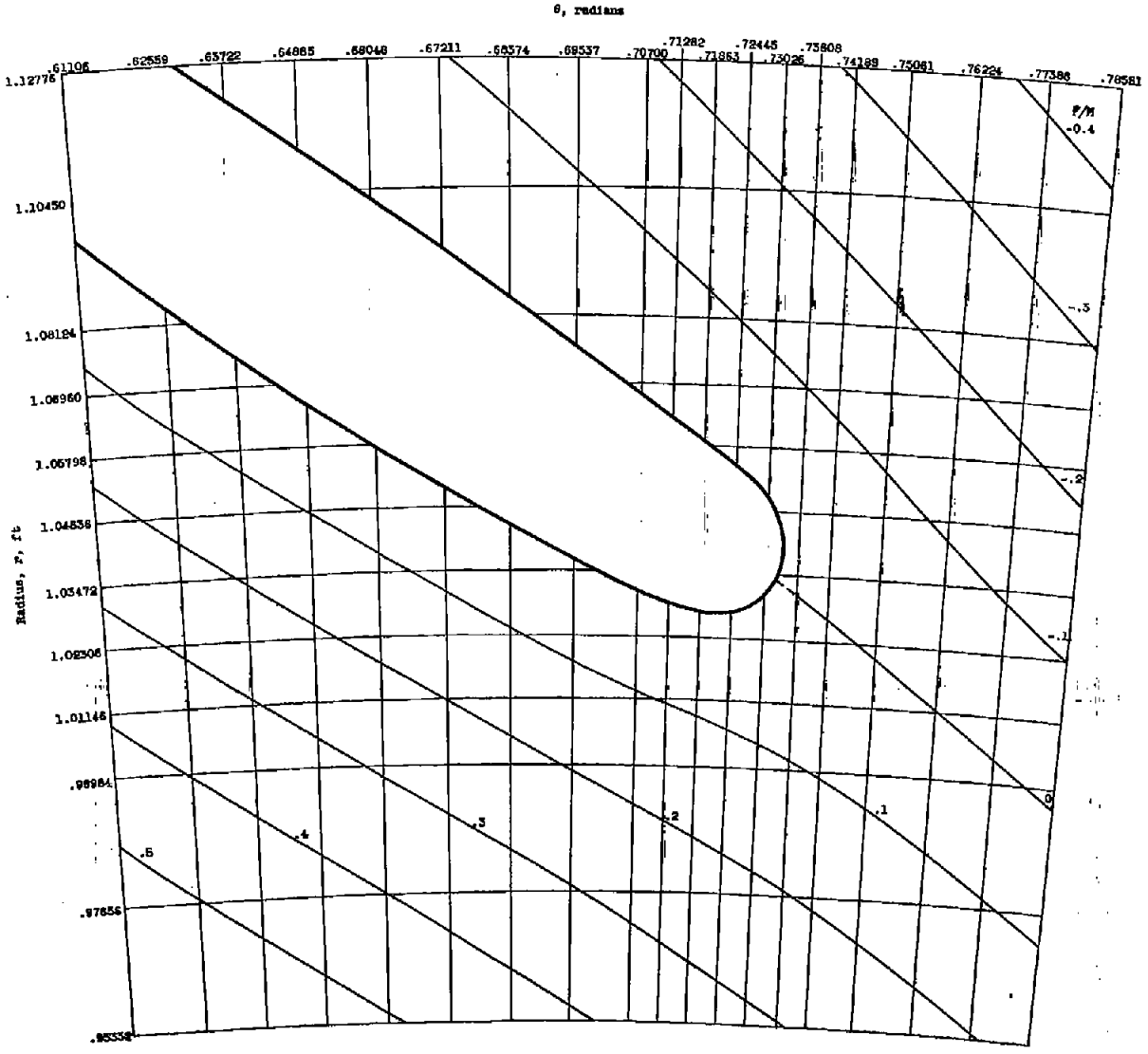

(c) Weight flow, 32.10 pounds per second (case C).

Figure 4. - Continued. Streamlines for refined solution in nose region.

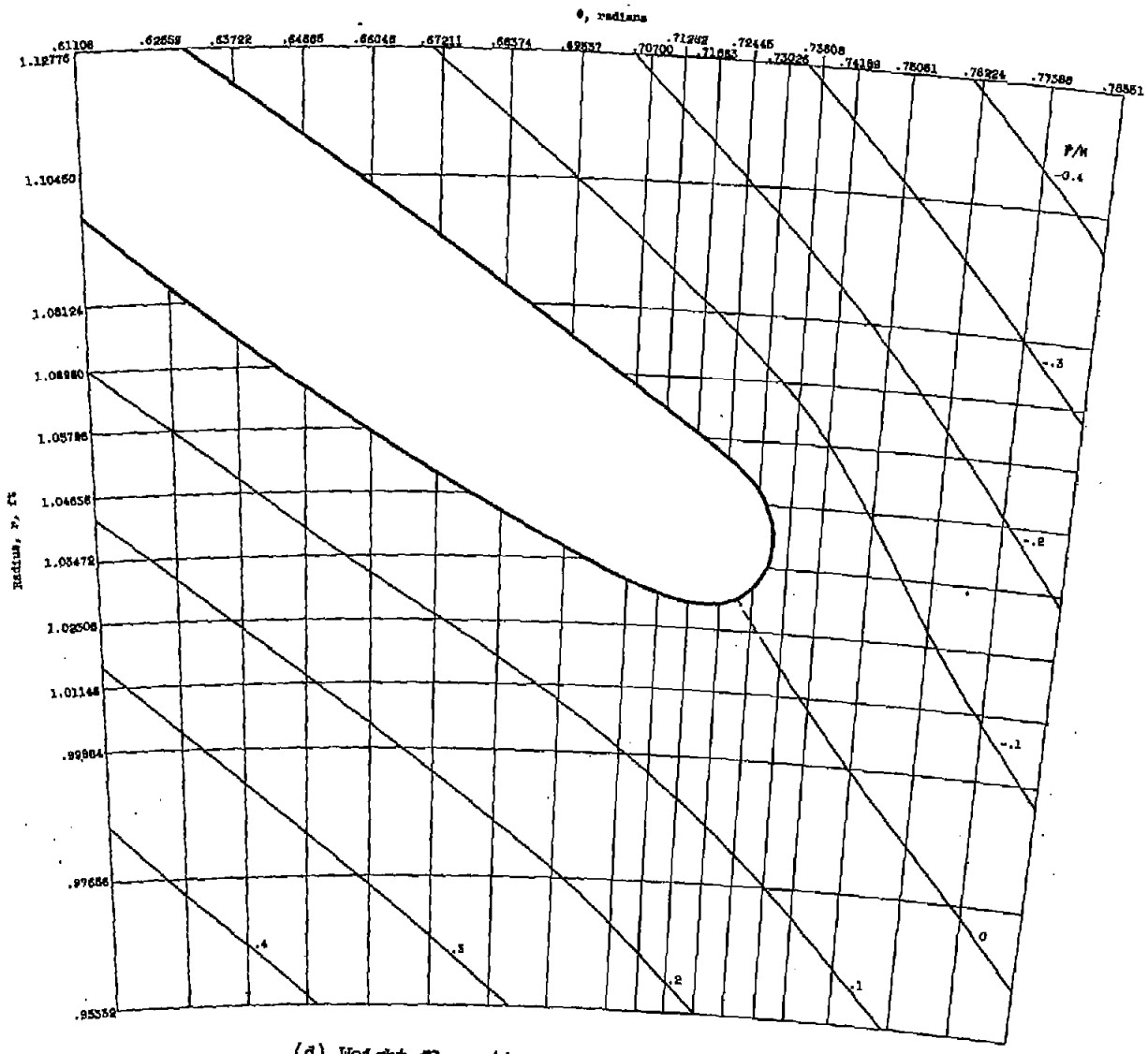

(d) Weight flow, 44 pounds per second (Case D).

Figure 4. - Concluded. Streamlines for refined solution in nose region.

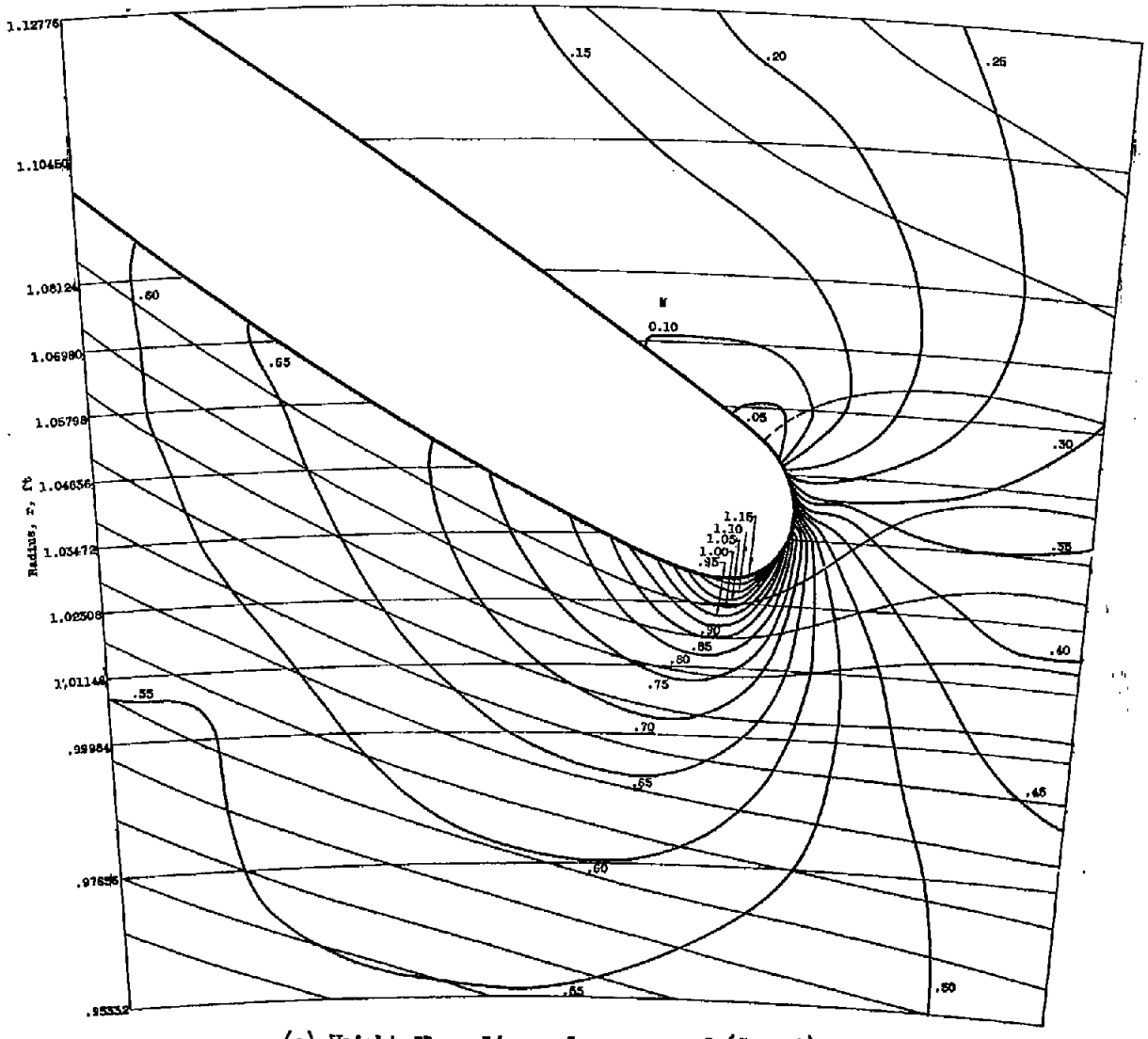

(a) Weight flow, 14 pounds per second (Case A).

Figure 5. - Contours of constant velocity ratio W for refined solution in nose region.

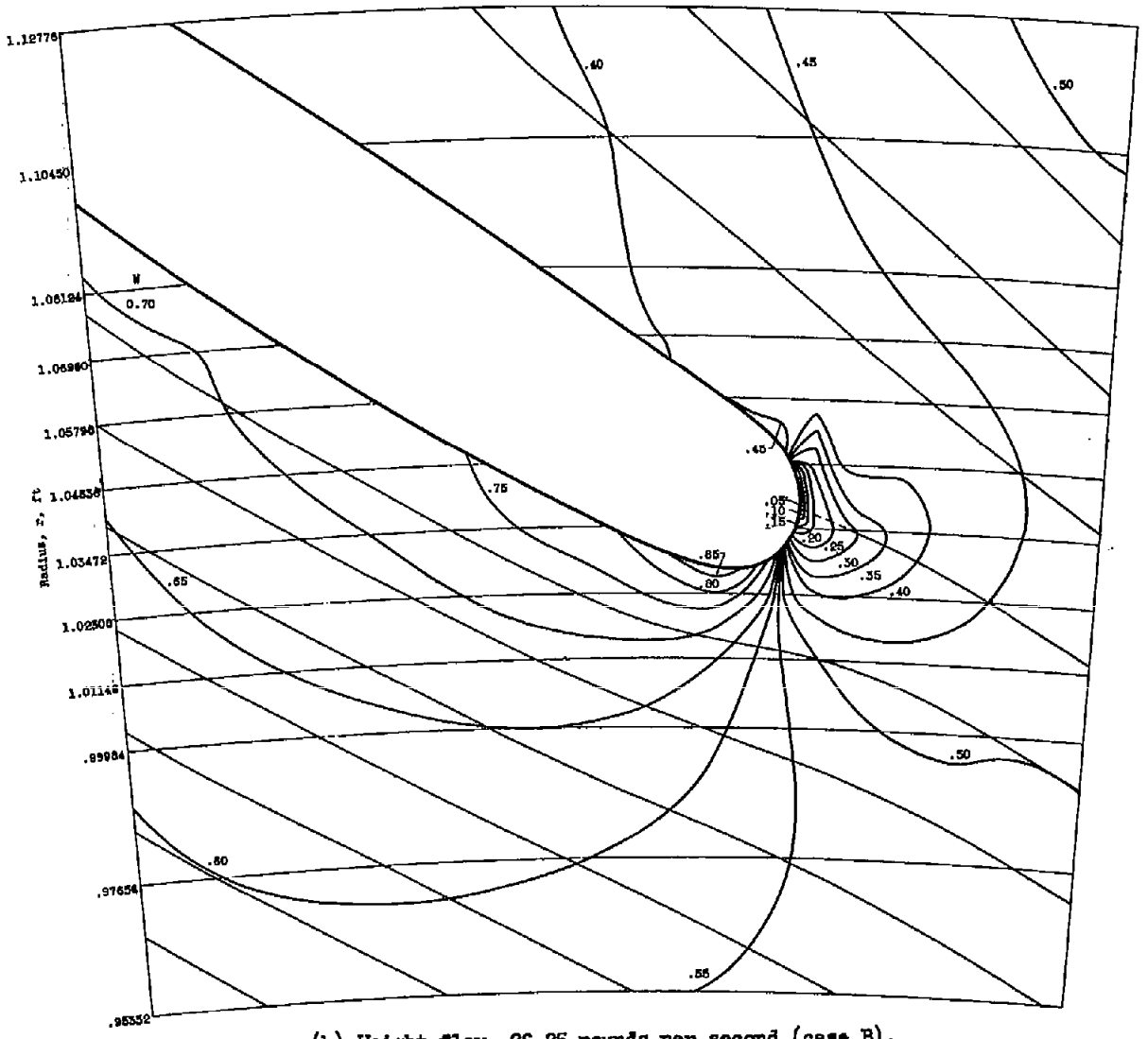

(b) Weight flow, 26.25 pounds per second (case B).

Figure 5. - Continued. Contours of constant velocity ratio W for refined solution in nose region.

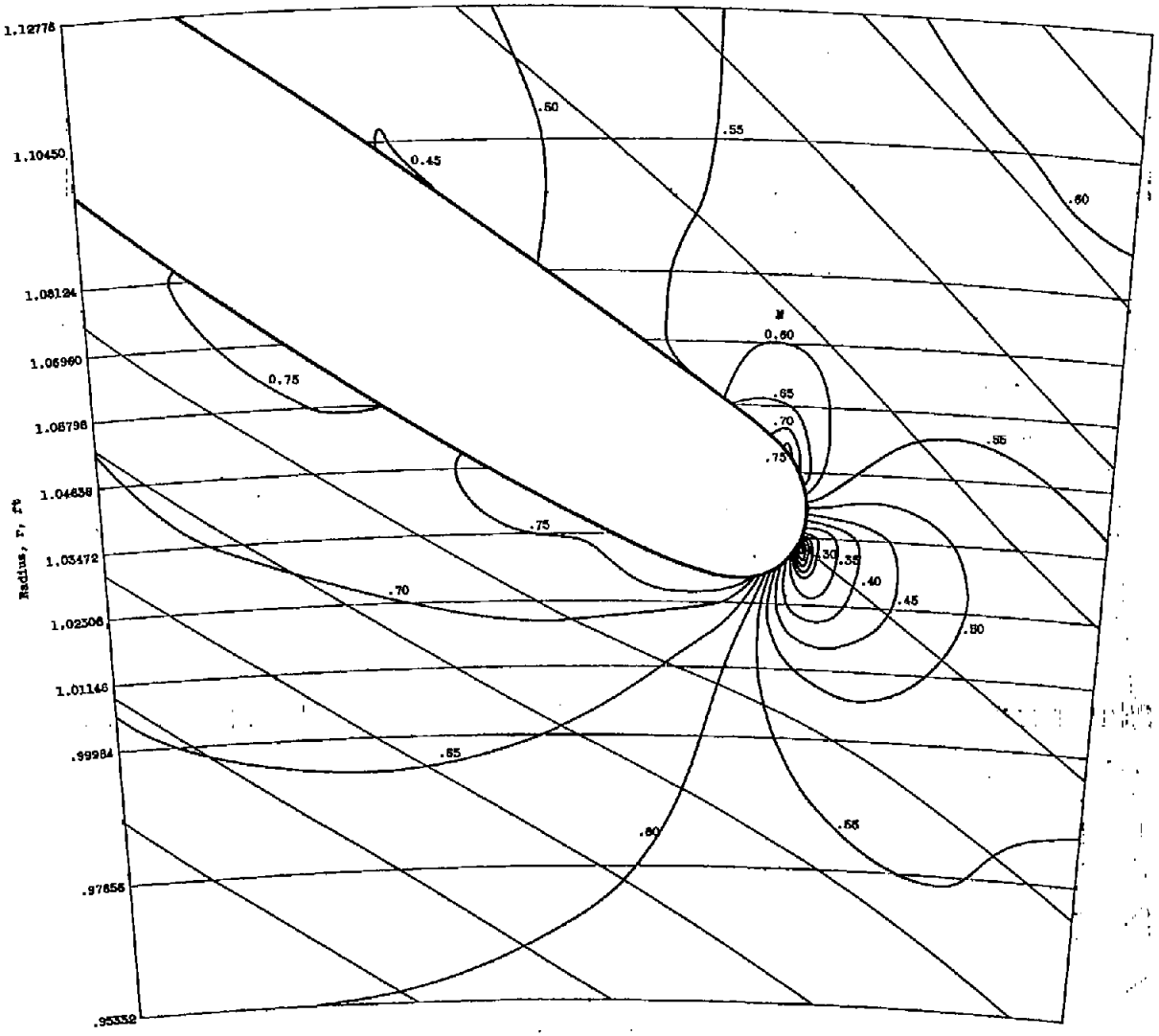

(c) Weight flow, 32.10 pounds per second (case C).

Figure 5. - Continued. Contours of constant velocity ratio W for refined solution in nose region.

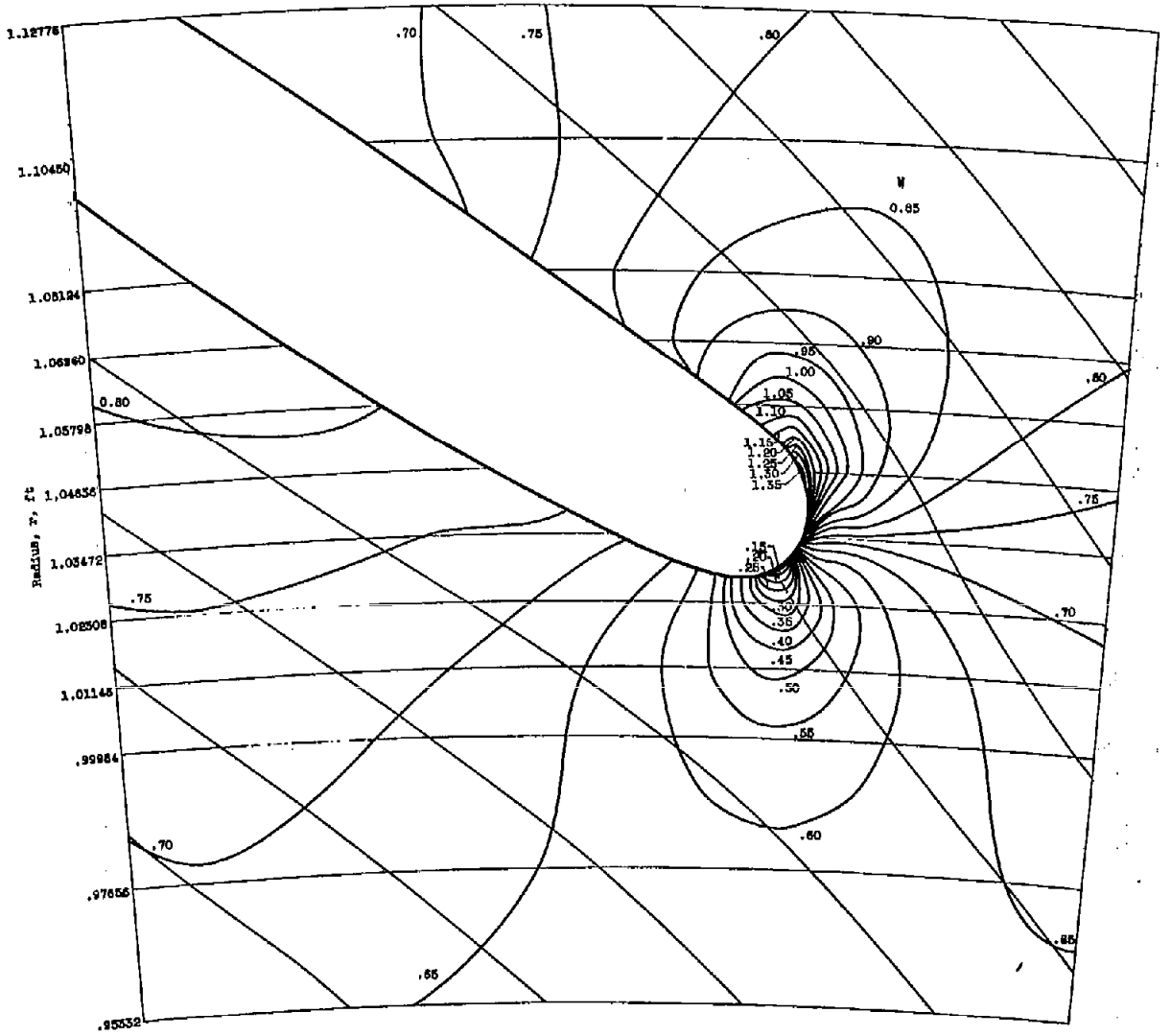

(d) Weight flow, 44 pounds per second (case D).

Figure 5. - Concluded. Contours of constant velocity ratio W for refined solution in nose region.